Journal of Materials Chemistry A

Accepted Manuscript

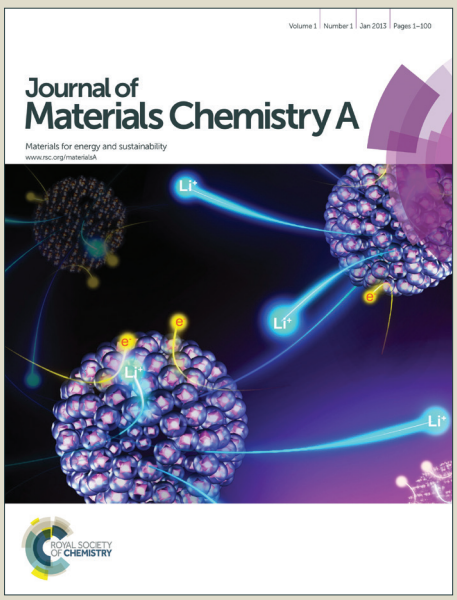

ROYAL SOCIETY OF CHEMISTRY

www.rsc.org/materialsA

Enhancement of Photovoltaic Performance of TiO_2-based Dye-sensitized Solar Cells by Doping $Ca_3La_{3(1-x)}Eu_{3x}(BO_3)_5$

W. B. Dai [a, *], Y. F. Lei [b], P. Li [c], L. F. Xu [d]

[a] State key laboratory of luminescent materials and devices, South China University of Technology, Guangzhou, Guangdong, China, 510640.
[b] State key laboratory for biological effects of nanomaterials and nanosafety, National Center for Nanoscience and Technology, Beijing, China, 100190.
[c] Guangzhou institute of energy conversion, Chinese Academy of Sciences, Guangzhou, Guangdong, China, 510640.
[d] School of materials science and engineering, South China University of Technology, Guangzhou, Guangdong, China, 510640.
[*] Author to whom correspondence should be addressed, E-mail: wubin.dai@foxmail.com

Abstract: A series of $Ca_3La_{3(1-x)}Eu_{3x}(BO_3)_5$ (CLBO: $3xEu^{3+}$) phosphors were prepared by the Pechini-type sol-gel technique. Rietveld refinement was performed by using the powder X-ray diffraction data, which shows occupation of Eu^{3+} on both Ca^{2+} and La^{3+} sites with a preferred location on the La^{3+} site over the Ca^{2+} site. In order to enhance the photovoltaic performance of dye-sensitized solar cells (DSSCs), a novel design is demonstrated by introducing CLBO: $3xEu^{3+}$ in TiO_2-based DSSC. As a new conversion luminescence medium, CLBO: $3xEu^{3+}$ transfers ultraviolet light to visible light via down-conversion, and increases the solar light harvest and photocurrent of DSSC. The experimental results reveal the feasibility of the conversion luminescence by doping rare-earth phosphors in the DSSC can provide an effective novelty way to improve the sunlight conversion efficiency for solar cells.

Keywords: Borates; Dye-sensitized solar cells (DSSCs); TiO_2; Dopants; Light-to-electric conversion

1. Introduction

Eu^{3+}-doped silicates, aluminates, aluminosilicates and derivatives are widely used in industry for their luminescent properties.[1] The emission of the Eu^{3+} ion typically consists of lines in red visible spectral area, which corresponds to transitions from the excited $^5D_0$ level to the ^7F_J (J = 0 to 6) levels of the $4f^6$ configuration. In some cases, those from higher 5D levels can also be observed depending on the host matrix (phonon frequency and the crystal structure) and the doping rate.[2, 3] Due to easy synthesis, good chemical stability and low-cost synthesis process, borates are of interest as host lattices (HLs) for doping different luminescent ions.[4, 5] Ultraviolet (UV) phosphors must have intense absorption in the UV range and high energy transfer (ET) efficiency from the HL to activator. Borates satisfy these conditions, since they show a proper forbidden band width.[6, 7] The crystal structure of the HL $Ca_3La_3(BO_3)_5$ (CLBO) has been determined previously.[8, 9] The structure consists of isolated BO_3 triangles and distorted [CaO_8] and [LaO_{10}] polyhedral, which are able to accommodate the luminescent ions and thus may serve as a HL for two-center luminescence (Fig.1b).

Solar energy has been considered as a green and inexhaustible energy source to fossil fuels.[10] Since a light-activation mechanism was applied to solar cells, dye-sensitized solar cells (DSSCs) have been developed and have shown great promise as a cost-effective alternative to traditional *p-n* junction silicon-based photovoltaic devices.[11, 12] Recently, nano-sized TiO_2 powders have been used as a working electrode for DSSCs due to a higher efficiency than any other metal oxide semiconductor.[13] However, the sensitized dyes practical used in DSSCs (i.e, N-719 or N-749 dye) only absorbs visible light, which induces the lower sun energy conversion efficiency.[14, 15] Therefore, it is necessary to enhance the conversion efficiency by extending the DSSCs absorption

range to longer or shorter wavelengths. By doping rare-earth (RE) phosphors and using luminescence down conversion mechanism, the UV light can be transferred into visible light and then reabsorbed by the sensitized dyes. Meanwhile, due to TiO_2 could act as sensitize center for emissions of Eu^{3+} ions (form a *p*-type doping and results in the elevation of Fermi level of the photoanode), doping with luminescent ions have been proved to be an excellent method for improving the quality of DSSCs.[13, 16]

In this study, different from other researches (i.e., Baker's group studied improving the light harvesting in DSSC via adding additional light scattering layer formed by silica / polymer nanocomposites[17] or increasing surface contact between electrolytes and photoanode[18]), doping element (Eu^{3+}) were designed to directly substitute the lattice Ti element, not to form a passive layer. Rather, fabricating a cell using combined surface area and charge-transfer enhancement by doping would be a more promising solution. Herein, we were undertaking a detailed study on the structure, optical properties of CLBO: 3xEu^{3+} phosphors and their applications in the TiO_2-based DSSC for improving the photovoltaic performance. One of the points of interest in this study is to find out the relationship between the Eu^{3+} dopant site(s) in the CLBO HL and its corresponding luminescence properties because it is not easy to deduce whether Eu^{3+} ions enter the La^{3+} or Ca^{2+} site or both owing to their different ionic radius and charge characteristics. Meanwhile, effects on the doped CLBO: 3xEu^{3+} phosphors (not only increases the photocurrent via conversion luminescence but also improves the photovoltage by *p*-type doping effect) were also investigated in TiO_2-based DSSC.

2. Experimental procedure

2.1. Sample preparations. Eu^{3+}-doped CLBO phosphors were prepared by the Pechini-type sol-gel technique.[19, 20] The doping concentrations of Eu^{3+} are 1-16 at.% of La^{3+}. Stoichiometric amounts of the reactants (RE_2O_3 (RE = La and Eu), H_3BO_3, $CaCO_3$) were dissolved in concentrated nitric acid, then citric acid was added to the solution. A citric acid to cation molar ratio of 1: 1 was employed to prepare the precursor solution. The precursors were dried at 150°C and fired at 1000°C for ~ 4h in air. After these processes, polycrystal powders were obtained. The colloid TiO_2 was obtained via previous method (the detailed process is described in Supporting information).[21, 22] The CLBO: $3xEu^{3+}$ powder was mixed into the colloid ultrasonically vibrating for 70 min and hydrothermally treating at 180°C for ~ 20h to form a mixed (CLBO: $3xEu^{3+}$ + TiO_2) colloid. A TiO_2 film (~ 12 μm) was obtained by coating the colloid on the FTO plate with sintered at 430°C for 25 min. Then, the doping layer of the mixed colloid (~ 3 μm) was coated on TiO_2 film in the same process (For transversal comparison, the 15 μm thick CLBO: $3xEu^{3+}$-doped TiO_2 photoelectrode was also fabricated in the same method). Afterwards, the film was soaked in dye N-719 for ~ 20h to form a dye-sensitized film electrode. In order to comparison, a dye-sensitized TiO_2 film electrode without CLBO: $3xEu^{3+}$ was also made, which has the same thickness as the film with CLBO: Eu^{3+} (~ 15 μm). The DSSC was assembled by injecting the electrolyte into the aperture between the dye-sensitized TiO_2 film electrode and a platinum counter electrode, which were clipped together.

2.2. Sample characterizations. The morphology was observed by a field emission scanning electron microscope (SEM, Hitachi S-4800, Tokyo, Japan) and elemental analysis was analyzed by using SEM-energy dispersive spectroscopy (EDS) system. XRD measurements were

performend on a D_8 Bruker diffractometer employing the Cu K_α radiation and a Vantec multigap detector in the 5 - 125° 2θ interval. Structure refinement was performed by adopting the Jana 2006 Beta version software,[23] using a Rietveld procedure with the fundamental parameter approach in the $P6_3mc$ space group (SG). The instrumental function was expressed in terms of the geometry of the diffractometer with the relevant parameters reported in Table S1. The XRD data for structure refinement were collected in the step scan mode with steps of 0.02° (2θ) and a measuring of 2s per step. Steady luminescence spectra UV-VIS were recorded on an Edinburgh FLS920 spectrofluorometer with a continuous 450W xenon lamp as the excitation resource and by single photon counting. Electrochemical experiments were performed on an electrochemical cell filled with an electrolyte solution, where a Pt counter electrode, a saturated colomel reference electrode and a working electrode were immersed. The capacitance-voltage curves and potentiodynamic current-applied potential curves were measured by employing an Electrochemical Workstation (CHI660C, Shanghai Chenhua Device Co. Ltd., China). The photovoltaic parameters of the DSSCs were characterized by measuring the J-V character curves by using a 150 W xenon lamp (LHX150, Zolix Co., Ltd, Beijing, China) with AM 1.5G filter (AM 1.5G-3P, Sciencetech Inc., London, ON, Canada). The power of the simulated light was calibrated to one sun (100 mW/cm^2) using a reference Si photodiode (PL-RC, Trusttech Co., Ltd, Beijing, China). The incident photo-to-electron conversion efficiency (IPCE) of DSSCs was measured by measuring the short circuit current under the incident monochromatic light which comes from a xenon lamp through a monochromator (Omni-λ500, Zolix Co., Ltd). Eletrochemical Impedance Spectroscopy (EIS) were recorded by the same workstation and the measurements were taken over a frequency range of 0.1-100 kHz under standard global AM1.5 solar irradiation.

3. Results and discussion

3.1. Crystal structure and optical properties. Fig. 1a shows the XRD patterns of CLBO: 3xEu^{3+} (3x = 0 to 16 at.%) phosphors, CLBO HL as well as the reported pattern of $Ca_3La_3(BO_3)_5$ in JCPDS (No. 31-0277). As an example, the particle image of the CLBO: 6%Eu^{3+} compound is shown in Fig.1c. Good particle distribution and rounded morphology is observed, which is of advantage to improve the emission intensity. All diffraction peaks of the samples were consistent with the JCPDS card which indicates the formation of pure single phases for all the samples. To further confirm the structure of the phosphors, Rietveld structure refinements were performed. Due to the cationic size of Eu^{3+} is smaller than La^{3+} and Ca^{2+} (for both the 10- and 8-coordinate number (*CN*)) in the CLBO HL, the occupancies of Eu^{3+} on both La^{3+} and Ca^{2+} sites were refined, which indicates the Eu^{3+} cations can both enter into the Ca^{2+} and La^{3+} sites. Eu^{3+} ions cannot occupy interstitial or B^{3+} sites due to the large differences in ionic radius. As listed in Table 1, with the increase of Eu^{3+} doping concentration, the lattice parameters (*a*, *c* and *V*) become smaller which further means the Eu^{3+} cations have been incorporated into the CLBO matrix. There are no La^{3+} cations entering into the Ca^{2+} site on all of the prepared samples, which indicates that it is the Eu^{3+} ions doping induce the antisite disorder in the CLBO: 3xEu^{3+} samples. The preferred occupancy of the Eu^{3+} ions on the La^{3+} site over the Ca^{2+} site is due to the fact that La^{3+} and Eu^{3+} ions have the same valence state and Eu^{3+} ions are closer to La^{3+} than Ca^{2+} ions by considering the chemical bonding. Fig. 1d shows the Rietveld fit of XRD pattern for the sample CLBO: 6%Eu^{3+} and Table S2 lists the refined lattice constants, the atomic and thermal parameters for the CLBO HL.

The photoluminescence excitation (PLE) and PL curves for the CLBO: 3xEu^{3+} ($0 \leq 3x \leq 16\%$)

phosphors are plotted in Fig. 2 at room temperature (RT). Except the undoped sample, the PL spectra for other samples show line peaks between ~ 570 and 720 nm because of the transitions from the lowest excited state $^5D_0$ to the ^7F_j levels (j = 0 to 4), while the PLE spectrum (curve a) is composed by two parts: i) the band located in the UV range is originated from the allowed charge transfer state (CTS) band (Eu^{3+}-O^{2-}) and ii), sharp peaks from ~ 310 to 530 nm are associated with typical intra-4f forbidden transitions. These sharp excitation bands that centered at ~ 320, 383, 393, 414, 463 and 526 nm are attributed to the $^7F_0 \rightarrow {}^5D_4$, $^7F_0 \rightarrow {}^5L_7$, $^7F_0 \rightarrow {}^5L_0$, $^7F_0 \rightarrow {}^5D_3$, $^7F_0 \rightarrow {}^5D_2$ and $^7F_0 \rightarrow {}^5D_1$ transitions, respectively.[24, 25] The intensity of the CTS band is much higher than the 4f-4f transitions in the excitation spectrum due to the allowed electronic transition from the 2p orbital of O^{2-} to the 4f orbital of Eu^{3+} *vs*. the forbidden transitions within the $4f^6$ configuration. The curves in the bottom of the Fig. 2 show the PL spectra of CLBO: 3xEu^{3+} under λ_{ex} = 254 nm excitation. The strongest peaks sited at ~ 625 and 708 nm are attributed to $^5D_0 \rightarrow {}^7F_2$ and $^5D_0 \rightarrow {}^7F_4$ transitions, respectively. Other peaks centered at ~ 580, 593 and 650 nm are assigned to the $^5D_0 \rightarrow {}^7F_0$, $^5D_0 \rightarrow {}^7F_1$ and $^5D_0 \rightarrow {}^7F_3$ transitions, respectively. Due to the valence electrons of Eu^{3+} ions are shielded by the 5s and 5p outer electrons and the 4f-4f transitions of Eu^{3+} ions are weakly affected by ligand ions, the line shape of emission curves do not change with the different Eu^{3+} ion doping concentration. The PLE spectra indicate that this kind of phosphors can be excited by UV light either indirectly through the CLBO HL or directly through absorption by Eu^{3+} ions themselves and emit visible light, which is overlapped with the absorption range of the N-719 dye. The PL intensity increases with Eu^{3+} doped concentration until a saturated intensity is reached (3x = 6%, critical concentration) under λ_{ex} = 254 nm. Hence, the doping rate of Eu^{3+} will be fixed at 6% for the electrochemical analysis in TiO_2-based DSSC.

Since the splitting of either $^5D_0$ and $^7F_0$ is not possible, [2] the presence of two peaks must be due to separate emissions from the two different sites $(Eu(La)^{3+}$ and $Eu(Ca)^{3+}$, curve c in the inset of Fig. 2). Namely, Eu^{3+} ions sited at both La^{3+} and Ca^{2+} sites, which is in good agreement with the result reported in Table 1. Actually, these peaks are always very weak or even altogether absent. However, in our case, both sites in the CLBO HL structure have low symmetry, which can be readily to relax the selection rules. The different Eu^{3+} sites explained why there are shoulder peaks on each line peak in PL spectra. According to the crystal field effect, which speculates the higher coordinate number (*CN*), the shorter the wavelength of the emission because of a lower crystal field splitting, we can expect that the peaks at ~ 578 nm and ~ 580.5 nm are originated from $Eu(La)^{3+}$ (10-*CN*) and $Eu(Ca)^{3+}$ (8-*CN*), respectively.

Because the smaller energy gaps between $^5D_{3,2,1}$ and $^5D_0$, which can be bridged by the vibration energies and manifested in the form of non-radiative process, emissions from the higher $^5D_{3,2,1}$ levels to the ground state were not observed in the PL spectra (if exists, the peaks should be also sharp in the shorter wavelengths). The non-radiative multi-phonon relaxation rate of the $4f^n$ Eu^{3+} configuration can be expressed by Equ. (1): [25, 26]

$$W_{NR} = W_{NR}(0)\exp(\alpha n\hbar\omega_p) \qquad (1)$$

where α depends on the character of the phonon, W_{NR} is the relaxation rate, $\hbar\omega_p$ is the highest available vibrational phonon energy, ΔE is the energy difference between the levels, $n = \Delta E / \hbar\omega_p$ is the number of phonons to fill the energy gap. According to Equ(1), a high maximum available phonon energy in the CLBO HL can reduce the number of phonons and thus fill the energy gap and enhance multi-phonon relaxation to bridge the energy level between $^5D_{3,2,1}$ and $^5D_0$. From this point of view, the excitation energy from one Eu^{3+} $^5D_{3,2,1}$ levels could promotes another nearly

Eu^{3+} ion from the ground state to the metastable state level, such as $^5D_1(Eu_1) + {}^7F_0(Eu_2) \rightarrow {}^5D_0(Eu_1) + {}^7F_3(Eu_2)$. As a result, the higher $^5D_{3,2,1}$ levels emission can be easily quenched via cross-relaxation and the $^5D_0$ emission becomes dominant. Based on these results, the UV irradiation can be absorbed by the N-719 dye in the TiO_2-based DSSC through down-conversion mechanism, which expects to widen the light absorption range of the DSSC.

3.2. Electrochemical analysis for CLBO: 6%Eu^{3+} doped in TiO_2 film. SEM images of pure and CLBO: 6%Eu^{3+} doped TiO_2 films are shown in Figs. 3a and 3b. The typical size of tightly interconnected TiO_2 nanoparticle is ~ 20 - 30 nm and most of the particle morphology is spherical. For the phosphor doped TiO_2 films, the nanoparticles shape is rod-like and the typical diameter and length of the nanorod are ~ 50 -100 and 250 - 450 nm, respectively. The presence of CLBO: 6%Eu^{3+} (6wt.%) elements in the doped TiO_2 films were analyzed by using EDS, as one can see in Fig. 3c. The estimated composition of the sample was given in Table 2.

The effects of CLBO: 6%Eu^{3+} on the energy level of TiO_2 is assessed via Mott-Schottky electrochemical analysis. Fig. 4a shows Mott-Schottky plots ($1/C^2$ *vs*. V) of the TiO_2 film with different amount of CLBO: 6%Eu^{3+}. According to the Mott-Schottky Equ. (2), [27, 28] the flat-band potential (V_{FB}) can be evaluated, which relates the capacity to the potential difference between the surface and the bulk of a semiconductor ΔV:

$$C^{-2} = \frac{2}{\varepsilon\varepsilon_0 e N_i}\left(Z_i \Delta V - \frac{KT}{e}\right) \quad (2)$$

where ε is the dielectric constant of the material, ε_0 is the permittivity of the vacuum, e is the element charge, N_i is the concentration of donors in *n*-type and acceptors in *p*-type semiconductor, Z_i is + 1 for donors and – 1 for acceptors. One can see a negative shift of the value V_{FB} with the increase of the amount of CLBO: 6%Eu^{3+} from -0.389 V for TiO_2 film to -0.874 V for the film

doped with CLBO: 6%Eu^{3+} of 8wt.% (Table 3). This result is due to the fact that the pristine TiO_2 film is a *n*-type semiconductor and the introduction of + 3 value (Eu^{3+}) metal ions into + 4 ones (Ti^{4+}) would induce a *p*-type doping effect that leads to the negative shift of the V_{FB} with the increase of CLBO: 6%Eu^{3+} amount in the TiO_2 film (the same process as the + 3 metal ions into + 4 ones in Si semiconductor). Note here, the doping different amount of CLBO: 6%Eu^{3+} cannot change the TiO_2 film semiconductor type. However, the doping rate can influence the Fermi level and the V_{FB} of the TiO_2 film.

The potentiodynamic parameters for different amount of CLBO: 6%Eu^{3+} (0 to 8 wt.%) compounds doped in TiO_2 films were also measured as one can see in Fig. 4b (current-potential curves). With the increase of the applied potential, one can observe that the insertion of CLBO: 6%Eu^{3+} in TiO_2 film triggers the photocurrent densities firstly increase and then gradually tend to a saturation value. Obviously, the photocurrent densities for the CLBO: 6%Eu^{3+} / TiO_2 system are all larger than the TiO_2 film (Table 3).

3.3. Photovoltaic performance of DSSCs. To investigate the photovoltaic characteristic of DSSCs under UV irradiation, optical filters were adopted to filter out the light, which the wavelength is larger than 350 nm. Fig. 4c exhibits the photovoltaic character curves for the DSSCs without and with CLBO: 6%Eu^{3+} (6wt.%) doping under an UV irradiative (24 mW/cm^2). The fill factor (*FF*) and light-to-electric energy conversion efficiency (η) were calculated according to the Equs. (3-4): [12]

$$FF = \frac{V_{\max} \times J_{\max}}{V_{OC} \times J_{SC}} \qquad (3)$$

$$\eta = \frac{V_{\max} \times J_{\max}}{P_{in}} \times 100\% = \frac{V_{OC} \times J_{SC} \times FF}{P_{in}} \times 100\% \qquad (4)$$

where J_{SC} is the short-circuit current density (in mA/cm^2), V_{OC} is the open-circuit voltage (V), P_{in} is the incident light power, and J_{max} (in mA/cm^2) and V_{max} (V) are the current density and voltage in the J-V curves at the point of maximum power output, respectively. The photovoltaic parameters of DSSC without CLBO: 6%Eu^{3+} doping are: J_{SC} = 1.184 mA/cm^2, V_{OC} = 0.577 V, FF = 0.530 and η = 0.367%, respectively. For the DSSC doped with CLBO: 6%Eu^{3+} (6wt.%) compound shows enhanced photovoltaic parameters: J_{SC} = 1.398 mA/cm^2, V_{OC} = 0.677 V, FF = 0.561 and η = 0.548%, respectively. These results indicate that UV light can be effectively converted to visible light by doping CLBO: 6%Eu^{3+} compound. Hence, for the doped sample, in some extent, the more incident light are absorbed, the higher efficiency of the DSSC.

The photocurrent-voltage curves of the DSSCs without and with different amount of CLBO: 6%Eu^{3+} doping under a simulated solar light irradiation (100 mW/cm^2) were shown in Fig. 4d and the photovoltaic parameters are listed in Table 4. From the experimental results, the values of V_{OC} increase with the increase of CLBO: 6%Eu^{3+} amount in the DSSC. The values of J_{SC} first increase till an concentration quenching (6 wt.%) and then decrease. The maximum efficiency of the DSSC (7.953%) is obtained when the amount of CLBO: 6%Eu^{3+} is 6 wt.% in the doping layer. For the J_{SC} values, before quenching (6wt.%), the increase can be attributed to the down-conversion luminescence of Eu^{3+} from UV light to visible light. Furthermore, the changes of TiO_2 film energy level can improve the carrier transport at the interface of TiO_2/dye, which helps in improving the J_{SC}. After the doping concentration quenching, perhaps more grain, phase and domain interfaces in the doping layer are created, which can capture photogenerated electrons and holes and result in impeding the charge carrier transportation and leading to decrease in photocurrent.[29, 30] For comparison, the photovoltaic performance of the 15 μm thick CLBO: 0.06Eu^{3+}-doped TiO_2

photoelectrode was shown in the ESI (Fig. S1).

Meanwhile, the V_{OC} is the difference between the Fermi level of the electrons in the oxide film and the redox potential of the electrolyte ($V_{OC} = E_{F(TiO2)} - E_{redox}$).[31] The changes in V_{OC} are due to the band-edge movement relative to the redox electrolyte energy. When Eu^{3+} cations were doped in the TiO_2 film, the Eu^{3+} ions will substitute in the Ti^{4+} ions lattice sites, which induce a *p*-type doping. Therefore, the conduction band edge of TiO_2 moves upward and the Fermi level improves, as a result, V_{OC} increases after the CLBO: 6%Eu^{3+} doping. As could be seen in Table 4, when the ratio of CLBO: 6%Eu^{3+} / TiO_2 is fixed at 6 wt.% in the doping layer, the light-to-electric energy conversion efficiency of the DSSC reaches to 7.653%, which is much higher than the DSSC without RE ion doping (by increasing ~35%). As different from other studies in this field (spectral converters by RE compound were installed on the front or the back in the TiO_2 film), we introduced doped RE compound (CLBO: 6%Eu^{3+}) in the doping layer (TiO_2 photoanode) of DSSC, that can enhance the effective conversion efficiency and *p*-type doping effect.

Fig.5a shows the IPCE spectra of DSSCs without and with Eu^{3+}-doped electrodes. In light range (300 – 800 nm), the largest IPCE was observed for DSSC with Eu^{3+}-doped (6wt.%) electrode and the IPCE of DSSC without Eu^{3+}-doped electrode is the lowest. The IPCE of DSSC depends on the incident light harvesting and light scattering.[32] Light harvesting effect is attributed to the surface area of TiO_2 and the dye adsorbed amount, and the light scattering effect is related to the shape of TiO_2. When light wavelength is larger than ~ 400 nm, the IPCE of DSSCs with Eu^{3+} (6wt.% and 2wt.%)-doped electrode is much larger than pure TiO_2 electrode. The shape and size of Eu^{3+}-doped (6wt.%) TiO_2 particles are almost the same as the one with Eu^{3+}-doped (2wt.%) TiO_2 particles (Fig.S2), and their light scattering contribution to DSSC efficiency should be also

almost the same. Therefore, we can indicate that a large efficiency improvement of DSSC with Eu^{3+}-doped electrode is mainly due to down-conversion luminescence effect rather than light scattering effecting.

To further analyze the impact of applying the Eu^{3+}-doped dyes to sensitize solar cell electrodes towards electron transportation processes at the interface, the Nyquist plots of EIS, measured at a bias voltage corresponding to the V_{oc} are presented in Fig.5b. The impedance of diffusion of redox species in the electrolyte is not negligible under illumination because the current flow in the cell is large. On the other hand, the Fermi level in TiO_2 approaches the lower edge of the conduction band, so the electron transport resistance is negligible.[33] The equivalent circuit is presented in the Fig.S3. As indicated in Fig.5b, three typical EIS spectra exhibit three semicircles in the Nyquist plot. In the order of increasing frequency the features are attributed to the Nernst diffusion in the electrolyte, electron transfer at the TiO_2/electrolyte interface, and redox charge transfer at the counter electrode, respectively. Under light illumination, the second semicircle radius in the Nyquist plot decreased after Eu^{3+}-doped N-719/TiO_2, and the values are in the order Eu^{3+}(6wt.%)-doped < Eu^{3+}(2wt.%)-doped < N-719, which indicates a decrease of the electron transfer impedance and an increase of charge transfer rate at the interface. The total resistance decrease is beneficial for electron transfer and further improving the performance of DSSCs. These results suggest that the high performances in TiO_2 based DSSC sensitized with Eu^{3+} are also due to the decrease of internal cell resistance.

4. Conclusion

In summary, through the Pechini-type sol-gel process, the pure phase of the phosphors CLBO: $3xEu^{3+}$ ($0 \leq 3x \leq 16\%$) were obtained and their photoluminescence properties were investigated. The PLE spectra of the CLBO: $3xEu^{3+}$ phosphors indicate that the Eu^{3+} ions can be excited by UV light, while the PL bands are just located in the absorption range of the N-719 dye. As a *p*-type dopant, Eu^{3+} ions elevate the Fermi level of the TiO_2 film and increase the photovoltage. When the doping amount of CLBO: $6\%Eu^{3+}$ is fixed at 6 wt.% in the doping layer, the light-to-electric energy conversion efficiency of the DSSC reaches to 7.953%, which is increased by ~ 35% compared to the TiO_2 film. These results demonstrate that the conversion luminescence in DSSC can provide an effective way to improve the sunlight conversion efficiency for solar cells.

5. Acknowledgement

This work is financially supported by the China Postdoctoral Science Foundation (Grant No: 2014M552019).

6. References

1. G. Denis, P. Deniard, E. Gautron, F. Clabau, A. Garcia, S. Jobic, *Inorg. Chem.*, 2008, **47**, 4226 - 4235.

2. G. Blass, B. C. Grabmaire, *Luminescent materials*. Springer-Verlag, 1994.

3. X. Liu, C. Li, Z. Quan, Z. Cheng, J. Lin, *J. Phys. Chem. C*, 2007, **111**, 16601 - 16607.

4. C. Liu, H. Liang, X. Kuang, J. Zhong, S. Sun, Y. Tao, *Inorg. Chem.*, 2012, **51**, 8802 - 8809.

5. Y. Zhang, Y. Li, Y. Yin, *J. Alloy. Compd.*, 2005, **400**, 222 - 226.

6. T. Jüstel, J. C. Krupa, D. U. Wiechert, *J. Lumin.*, 2001, **93**, 179 - 189.

7. I. E. Kwon, B. Y. Yu, H. Bae, Y. J. Hwang, T. W. Kwon, C. H. Kim, C. H. Pyun, S. J. Kim, *J. Lumin.*, 2000, **87**, 1039 - 1041.

8. Y. Zhang, J. K. Liang, X. L. Chen, M. He, T. Xu, *J. Alloy. Compd.*, 2001, **327**, 96 - 99.

9. T. Zhou, N. Ye, *Acta Cryst.*, 2008, **E64**, i37.

10. T. R. Cook, D. K. Dogutan, S. Y. Reece, Y. Surendranath, T. S. Teets, D. G. Nocera, *Chem. Rev.*, 2010, **110**, 6474 - 6502.

11. B. O'Regan, M. Gratzel, *Nature*, 1991, **353**, 737 - 740.

12. A. Hagfeldt, G. Boschloo, L. Sun, L. Kloo, H. Pettersson, *Chem. Rev.*, 2010, **110**, 6595 - 6663.

13. M. Durr, A. Bamedi, A. Yasuda, G. Nelles, *Appl. Phys. Lett.*, 2004, **84**, 3397 - 3399.

14. J. Wu, J. Wang, J. Lin, Y. Xiao, G. Yue, M. Huang, Z. Lan, Y. Huang, L. Fan, S. Yin, T. Sato, *Sci. Rep.*, 2013, **3**, 2058 - 2063.

15. S. H. Huang, *J. Am. Chem. Soc.*, 2013, **96**, 3108 - 3113.

16. W. Q. Liu, D. X. Kou, M. L. Cai, L. H. Hu, S. Y. Dai, *Prog. Chem.*, 2012, **24**, 722 - 736.

17. W. Yuan, H. Zhao, H. Y. Hu, S. Wang, G. L. Baker, *ACS Appl. Mater. Inter.*, 2013, **5**, 4115 –

4161.

18. W. Yuan, H. Zhao, G. L. Baker, *Org. Electron.*, 2014, **15**, 3362 – 3369.

19. M. P. Pechini, *Method of preparing lead and alkaline earth titanates and niobates and coating method using the same to form a capacitor*, U. S. Pat. 1967, No. 3330697.

20. M. Kakihana, M. Yoshimura, *B. Chem. Soc. Jpn.*, 1999, **72**, 1427 - 1443.

21. J. Wu, J. Wang, J. Lin, Z. Lan, Q. Tang, M. Huang, Y. Huang, L. Fan, Q. Li, Z. Tang, *Adv. Energy Mater.*, 2012, **2**, 78 - 81.

22. J. H. Wu, Z. Lan, J. M. Lin, M. L. Huang, S. C. Hao, T. Sato, S. Yin, *Adv. Mater.*, 2007, **19**, 4006 - 4011.

23. V. Petricek, M. Dusek, L. Palatinus, *The Crystallographic Computing System JANA*, 2006 Beta. Academy of Sciences: Praha, Czeck Republic, 2006.

24. W. B. Dai, M. Zhou, Z. Y. Xian, L. K. Zeng, *RSC Adv.*, 2014, **4**, 25470 - 25478.

25. Y. C. Chang, C. H. Liang, S. A.Yan, Y. S. Chang, *J. Phys. Chem. C*, 2010, **114**, 3645 - 3652.

26. S. Shionoya, W. M. Yen, *Phosphor Handbook*, CRC Press: Boca Raton, 1999.

27. L. G. Arriaga, A. M. Fernández, *Int. J. Hydrogen Energ.*, 2002, **27**, 27 - 31.

28. D. Hwang, J. Kim, T. Park, J. Lee, *Catal. Lett.*, 2002, **80**, 53 - 57.

29. K. H. Ko, Y. C. Lee, Y. J. Jung, *J. Colloid Interf. Sci.*, 2005, **283**, 482 - 487.

30. K. Murakoshi, G. Kano, Y. Wada, S. Yanagida, H. Miyazaki, M. Matsumoto, S. Murasawa, *J. Electroanal Chem.*, 1995, **396**, 27 - 34.

31. G. Schlichthörl, S. Y. Huang, J. Sprague, A. J. Frank, *J. Phys. Chem. B*, 1997, **101**, 8141 - 8155.

32. H. Koo, J. Park, B. Yoo, K. Yoo, K. Kim, N. Park, *Inorg. Chim. Acta.*, 2008, **361**, 677 – 683.

33. F. Fabregat-Santiago, J. Bisquert, G. Garcia-Belmonte, G. Boschloo, A. Hagfeldt, *Sol. Energy Mater. Sol. Cells*, 2005, **87**, 117 – 131.

Figures:

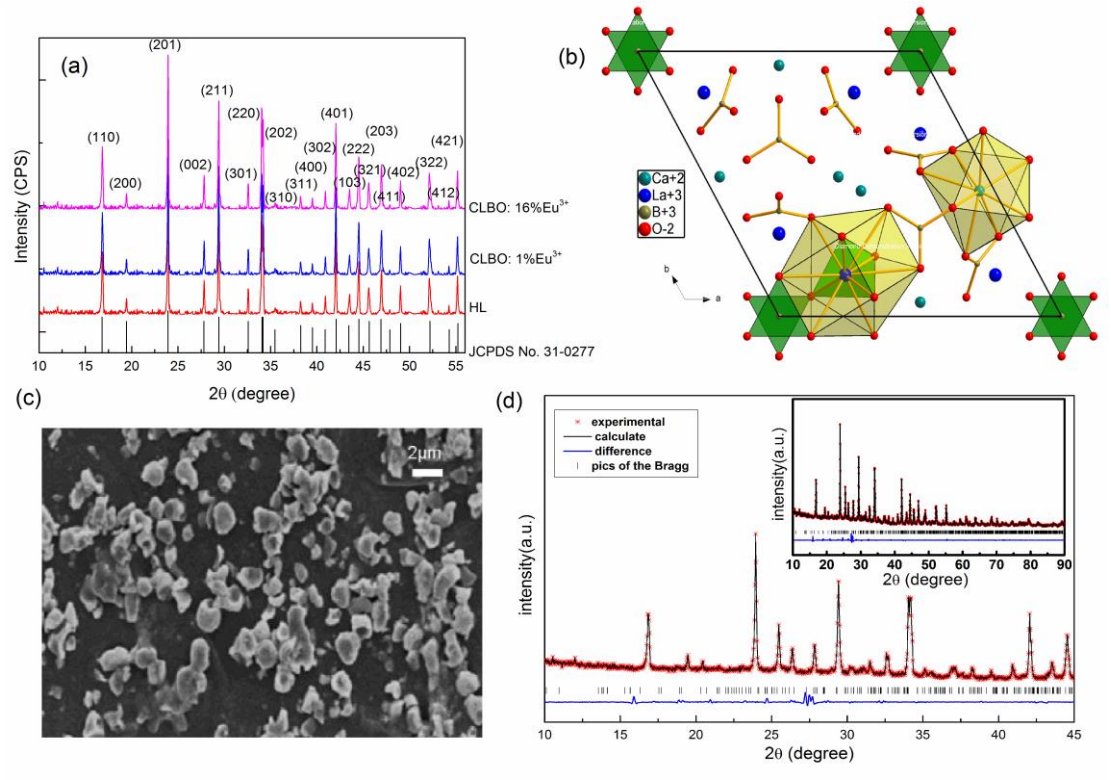

Fig.1. a), XRD patterns of CLBO: 3xEu^{3+} samples, b) crystal structure of CLBO along the [001] plane, the unit cell is consisted of [CaO_8] and [LaO_{10}] polyhedral and BO_3 triangles, c) SEM image of CLBO: 6%Eu^{3+} phosphor and d), observed, calculated and difference X-ray diffraction pattern of the CLBO: 6%Eu^{3+} in the [10-45] 2θ range (in inset is given the total pattern).

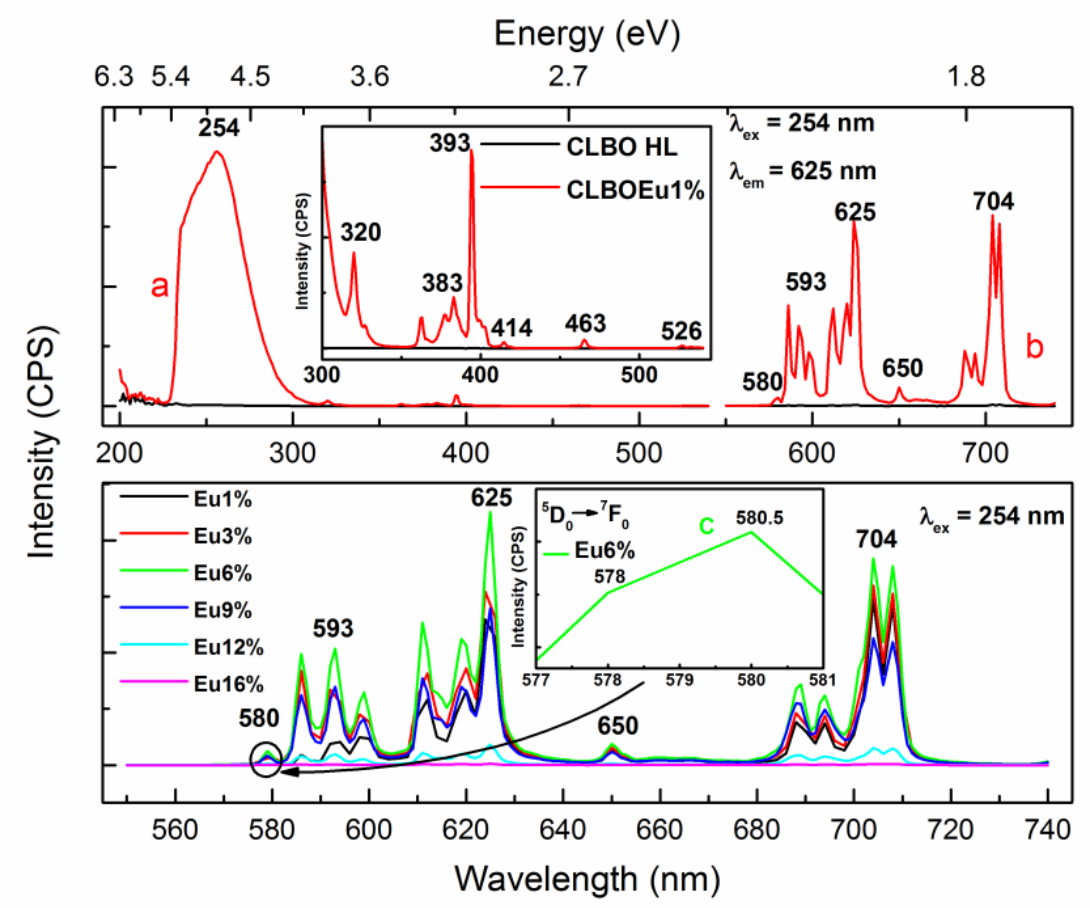

Fig.2. (Top) PL and PLE spectra of the CLBO HL and CLBO: 1%Eu^{3+} under λ_{ex} = 254 and λ_{em} = 611 nm, the inset shows the enlarged region of the PLE spectra between 300 and 530 nm. (Bottom) PL spectra of CLBO: 3xEu^{3+} ($1 \leq 3x \leq 16\%$) under λ_{ex} = 254, the inset shows the magnified area for the transition $^5D_0 \rightarrow {}^7F_0$ located at ~ 580 nm.

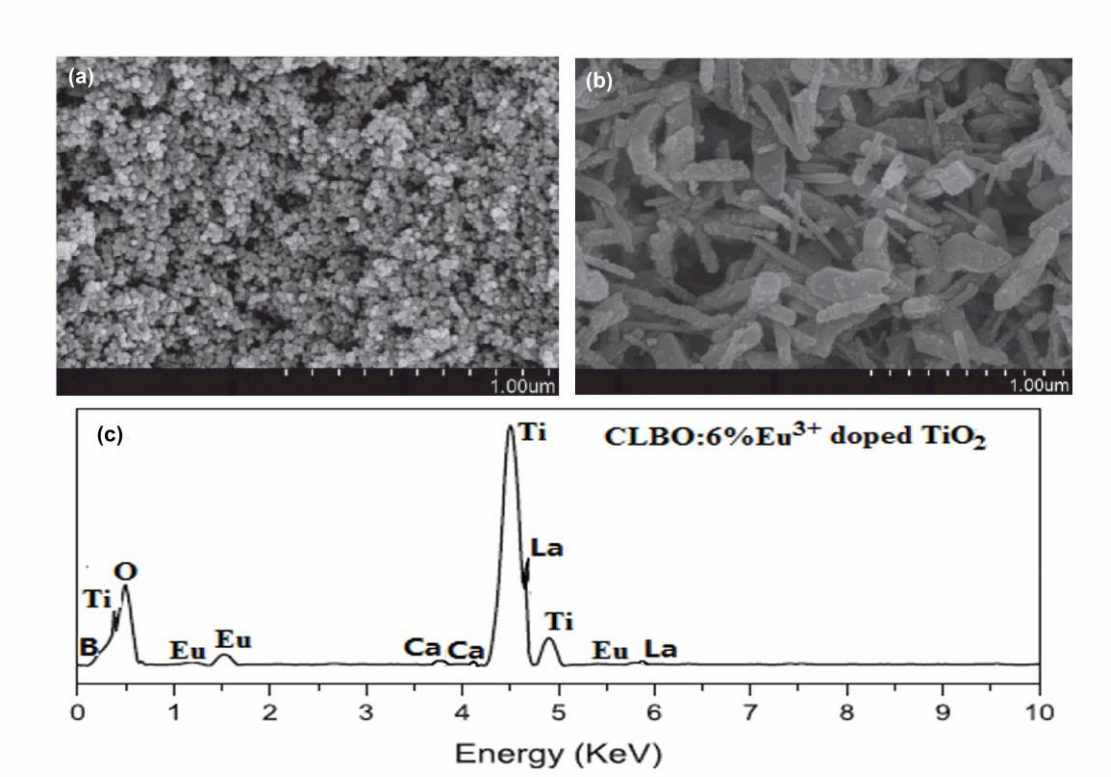

Fig.3. a), SEM image of undoped TiO_2 film, b), SEM image of CLBO: 6%Eu^{3+} (6wt.%) doped in TiO_2 film and c), EDS spectra of CLBO: 6%Eu^{3+} (6wt.%) doped in TiO_2 film.

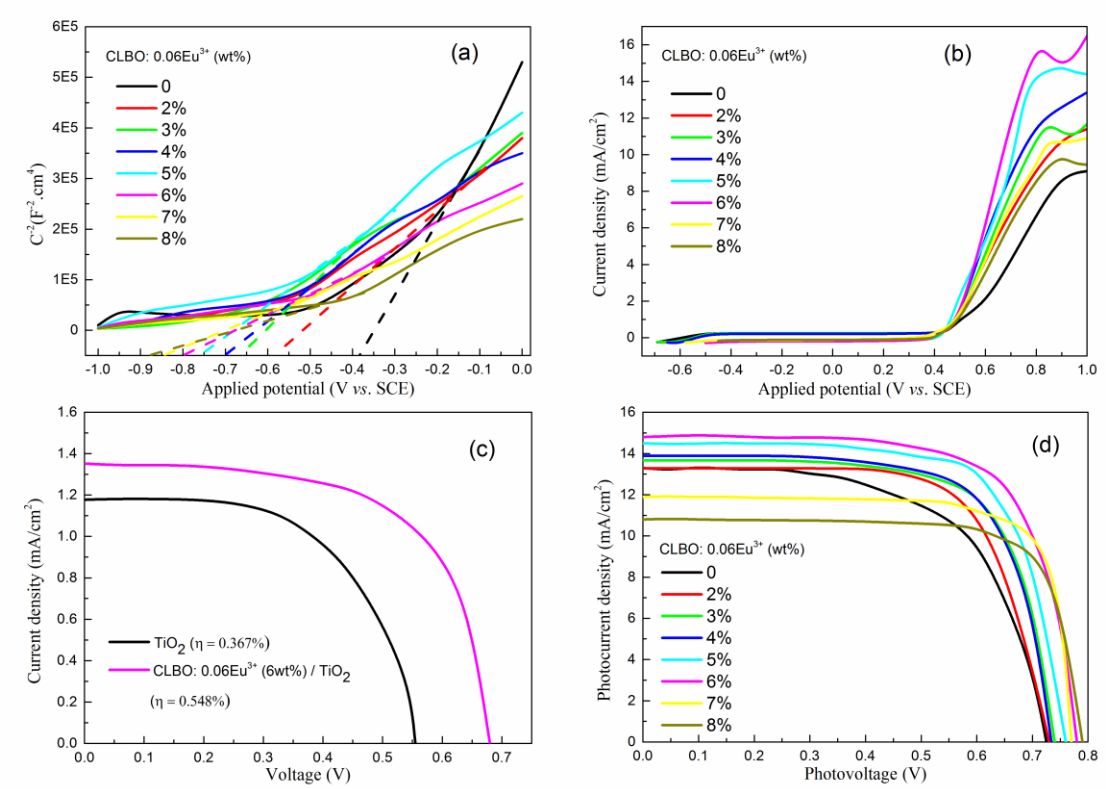

Fig.4. a) Mott-Schottky plots of CLBO: 6%Eu^{3+} / TiO_2 systems, b) current-potential curves, c) *J-V* curves of DSSC without and with CLBO: 6%Eu^{3+} doping (6wt%) under an UV light irradiation (24 mW/cm^2) and d), *J-V* curves of the DSSC contains different amount of CLBO: 6%Eu^{3+} doping under a simulated solar light irradiation (100 mW/cm^2).

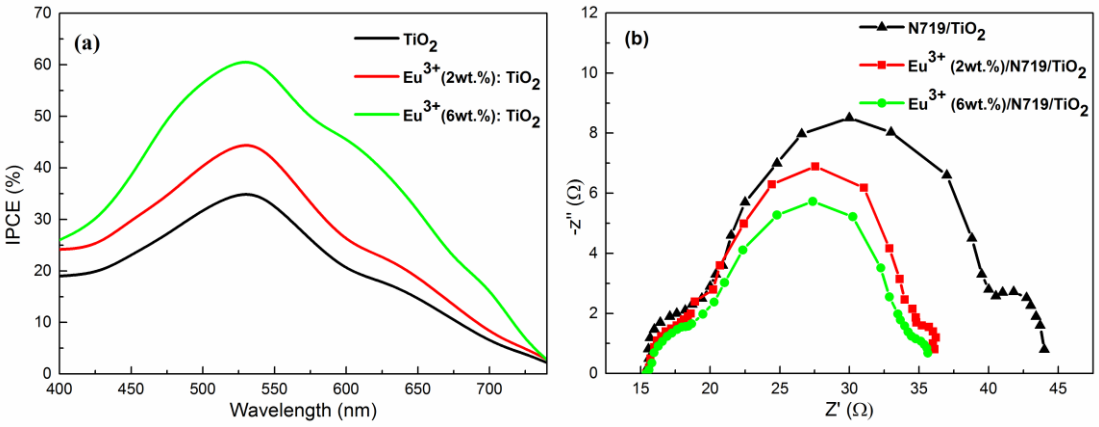

Fig.5. a)IPCE spectra of DSSCs based on single N719 sensitized and Eu^{3+} co-sensitized photoelectrodes, b) Nyquist plots of electrochemical impedance spectroscopy measured under standard AM 1.5G solar irradiation.

Tables:

Table 1 Crystallographic data and structure parameter of CLBO and its different doping rate of Eu^{3+} derivations.

Sample	CLBO HL	CLBO:1 %Eu^{3+}	CLBO:3 %Eu^{3+}	CLBO:6 %Eu^{3+}	CLBO:9 %Eu^{3+}	CLBO:12 %Eu^{3+}	CLBO:16 %Eu^{3+}
Occupancy of Ca^{2+}/Eu^{3+} on the Ca^{2+} site [a]							
Ca^{2+}	1	0.999(2)	0.994(1)	0.985(2)	0.979(2)	0.968(2)	0.961(2)
Eu^{3+}	0	0.001(1)	0.009(1)	0.014(2)	0.026(1)	0.030(1)	0.039(1)
Occupancy of La^{3+}/Eu^{3+}/Ca^{2+} on the La^{3+} site							
La^{3+}	1	0.992(2)	0.971(1)	0.929(1)	0.892(2)	0.869(1)	0.832(1)
Eu^{3+}	0	0.008(1)	0.022(2)	0.051(2)	0.067(1)	0.094(1)	0.121(2)
Ca^{2+}	0	0.001(1)	0.008(1)	0.017(2)	0.026(1)	0.029(1)	0.038 (1)
Lattice parameters							
a(Å)	10.530(1)	10.528(1)	10.526(2)	10.522(3)	10.521(2)	10.518(2)	10.511(2)
c(Å)	6.398(1)	6.397(2)	6.394(2)	6.391(3)	6.388(3)	6.381(3)	6.373(2)
V($Å^3$)	614.56(30)	614.47(20)	614.06(30)	613.55(30)	612.64(20)	611.27(30)	610.52(30)
Reliability factor							
R_{wp}(%)	3.66	3.45	3.61	3.69	3.61	3.58	3.54
R_p(%)	2.57	2.23	2.49	2.56	2.51	2.44	2.55
R_B(%)	0.67	0.61	0.69	1.01	0.78	0.66	0.72

[a] the occupation of Eu^{3+} on Ca^{2+} site would induce partial Ca^{2+} ions coming into La^{3+} site due to the whole charge balance in the CLBO HL. The possible antisite disorder among Eu^{3+}, La^{3+} and Ca^{2+} need to be considered during the refinement process.

Table 2 EDS estimated compositions of TiO_2 and CLBO: 6%Eu^{3+} doped TiO_2 nanoparticles.

Nominal doping rate (wt.%)	Titanium (at.%)	Oxygen (at.%)	Europium (at.%)	Calcium (at.%)	Lanthanum (at.%)	Boracium (at.%)
0	34.566	65.434	0	0	0	0
6	28.312	65.543	0.033	2.136	2.014	1.782

Table 3 Flat-band potential and saturated current density for CLBO: 6%Eu^{3+} / TiO_2 systems.

wt.%	0	2	3	4	5	6	7	8
V_{FB}[a]	-0.389	-0.572	-0.656	-0.698	-0.752	-0.798	-0.838	-0.874
I_{SAT}[b]	8.924	11.011	11.437	12.285	14.756	15.694	10.668	9.778

[a, b] data obtained from the Figs. 3a and 3b, respectively.

Table 4 Photovoltaic properties of the DSSCs doped with different amount of CLBO: 6%Eu^{3+}.

wt.%	V_{OC} (V)	J_{SC} (mA/cm^2)	*FF*	η (%)
0	0.724	13.209	0.596	5.832
2	0.730	13.288	0.624	6.436
3	0.735	13.626	0.657	6.841
4	0.739	13.930	0.678	7.277
5	0.761	14.459	0.685	7.556
6	0.782	14.801	0.692	7.953
7	0.781	11.889	0.706	5.872
8	0.789	10.826	0.713	5.636